

XMM–Newton observations of high-luminosity radio-quiet quasi-stellar objects

K. L. Page,^{1*} J. N. Reeves,² P. T. O’Brien,¹ M. J. L. Turner¹ and D. M. Worrall³

¹*X-Ray and Observational Astronomy Group, Department of Physics and Astronomy, University of Leicester, Leicester LE1 7RH*

²*Laboratory for High Energy Astrophysics, Code 662, NASA Goddard Space Flight Center, Greenbelt, MD 20771, USA*

³*H.H. Wills Physics Laboratory, University of Bristol, Bristol BS8 1TL*

Accepted 2004 May 20. Received 2004 April 30; in original form 2004 January 12

ABSTRACT

XMM–Newton observations of five high-luminosity radio-quiet quasi-stellar objects (QSOs; Q 0144–3938, UM 269, PG 1634+706, SBS 0909+532 and PG 1247+267) are presented. Spectral energy distributions were calculated from the *XMM–Newton* European Photon Imaging Camera (EPIC) and Optical Monitor (OM) data, with bolometric luminosities estimated in the range from 7×10^{45} to 2×10^{48} erg s⁻¹ for the sample, peaking in the ultraviolet. At least four of the QSOs show a similar soft excess, which can be well modelled by either one or two blackbody components, in addition to the hard X-ray power law. The temperatures of these blackbodies (~ 100 – 500 eV) are too high to be direct thermal emission from the accretion disc, so Comptonization is suggested. Two populations of Comptonizing electrons, with different temperatures, are needed to model the broad-band spectrum. The hotter of these produces what is seen as the hard X-ray power law, while the cooler (~ 0.25 – 0.5 keV) population models the spectral curvature at low energies. Only one of the QSOs shows evidence for an absorption component, while three of the five show neutral iron emission. Of these, PG 1247+267 seems to have a broad line (with an equivalent width of ~ 250 eV), with a strong, associated reflection component ($R \sim 2$), measured out to 30 keV in the rest frame of the QSO. Finally, it is concluded that the X-ray continuum shape of active galactic nuclei remains essentially constant over a wide range of black hole mass and luminosity.

Key words: galaxies: active – X-rays: galaxies.

1 INTRODUCTION

The X-ray continuum in Seyfert galaxies has been well studied; in these objects, a hard spectral component dominates the emission above ~ 2 keV. A proposed origin for this component is in a hot corona above the accretion disc surface, in which optical/ultraviolet (UV) photons from the disc are Comptonized to X-ray energies. A fraction of the hard X-ray power-law continuum then illuminates the disc (and possibly a molecular torus); some of these photons are absorbed, forming an iron K-edge at >7 keV, while others are reprocessed into an Fe K α line at 6.4 keV and a Compton reflection ‘hump’, caused by Compton down-scattering of the hard X-ray photons (Pounds et al. 1990).

It has been found that, although these features are generally observed in Seyfert 1 galaxies (Nandra & Pounds 1994), they are less common in the spectra of quasi-stellar objects (QSOs; e.g. Reeves et al. 1997; Lawson & Turner 1997). In many cases this could be related to a lack of signal-to-noise, but it is important to determine

whether such features are ubiquitous in QSOs and, hence, whether this emission mechanism is common over the full range of active galactic nuclei (AGN) luminosities. Observing the most luminous QSOs allows an investigation into objects where the accretion rate may be close to the Eddington limit and/or where the black hole mass may be large (i.e. $\sim 10^9 M_{\odot}$).

Work with *ASCA* (e.g. Reeves & Turner 2000) found evidence for iron-line emission in a number of QSOs, but often originating from ionized material, rather than the cold emission found for Seyferts. If this were true in general, it could be explained by the more luminous AGN having a higher accretion rate, which causes the surface of the disc to become ionized.

The QSOs in this paper form a small sample of high-luminosity, radio-quiet objects, with X-ray luminosities from 7×10^{44} to 3×10^{46} erg s⁻¹ (bolometric luminosities of 7×10^{45} to 2×10^{48} erg s⁻¹); the redshifts cover a range from 0.244 up to 2.038. Radio-quiet objects form the majority of luminous AGN (e.g. Kukula et al. 1998), but are less X-ray luminous than their radio-loud counterparts, for a given optical luminosity (Zamorani et al. 1981; Worrall et al. 1987; Wilkes et al. 1994). Because radio-quiet QSOs (RQQs) are fainter in the X-ray band, the high throughput of the *XMM–Newton* X-ray

*E-mail: kpa@star.le.ac.uk

telescopes makes the European Photon Imaging Camera (EPIC) instruments ideal for an X-ray investigation of distant RQQs. The aim of this study is to investigate the properties of the central engine in some of the most luminous QSOs (i.e. the extreme end of the accretion rate, black hole mass and/or luminosity parameter space). It is possible to do this with RQQs because the jet is thought not to contribute significantly to the X-ray emission, whereas, in radio-loud quasars, synchrotron or inverse Compton emission from a relativistic jet may dilute some of the spectral features (such as the iron line or soft excess) which are thought to originate from the accretion disc.

2 XMM-NEWTON OBSERVATIONS

Table 1 lists the dates and the instrumental set-up for each of the EPIC observations, while Table 2 gives the redshifts, Galactic absorbing column and radio measurements for each of the QSOs. A value of $R_L < 1$ defines the AGN as being radio-quiet, where R_L is given by the log of the ratio of the radio (5 GHz) to optical (B -band) fluxes (Wilkes & Elvis 1987; Kellerman et al. 1989).

The pipeline-produced event-lists were filtered using XMMSELECT within version 5.4 of the SAS (Science Analysis Software); single- and double-pixel events (patterns 0–4) were used for the PN, while patterns 0–12 were chosen for the MOS instruments. Spectra were extracted within a small circular region, centred on the source, with a radius of between 25 and 40 arcsec, depending on the source brightness. (Smaller regions were used for the fainter sources, to minimize the contribution from the background.) Background spectra (within the same size, or larger, region) were produced from an off-set position free of other sources. MOS 1 and MOS 2 spectra were subsequently co-added, after confirmation that the results were consistent. Source and background light curves were also extracted for each object. Time intervals of relatively high, flaring background were identified for both of the PG QSOs, and these periods were ex-

cluded from the following analysis. None of the source light curves showed variability over the duration of the observations after the removal of the background, however. After grouping the spectra to obtain a minimum of 20 counts per bin, version 11.1.0 of XSPEC was used to analyse the data. The most recent (time-dependent) response matrices (rmfs) were used when fitting the spectra, together with an ancillary response file (arf) generated by running ARFGEN within the SAS. The rmfs take into account the degradation of the instruments over the years since launch, and specifically model how the charge transfer inefficiency (CTI) has changed. Optical/UV magnitudes were obtained from the Optical Monitor (OM) where possible and these are discussed in Section 4. Errors are given at the 90 per cent level (e.g. $\Delta\chi^2 = 4.6$ for two interesting parameters). Throughout this paper, a *Wilkinson Microwave Anisotropy Probe* (WMAP) cosmology of $H_0 = 70 \text{ km s}^{-1} \text{ Mpc}^{-1}$, cosmological constant $\Omega_\lambda = 0.73$ and $\Omega_m = 1 - \Omega_\lambda$ is assumed; for comparison with previous conventions, using $q_0 = 0.1$ and $H_0 = 70 \text{ km s}^{-1} \text{ Mpc}^{-1}$ would give slightly smaller luminosity distances: a factor of $\sim 0.93\text{--}0.97$ ($z = 0.244\text{--}2.038$) compared to the values used here.

3 ANALYSIS OF EPIC DATA

3.1 The iron K band

Throughout the analysis, the co-added MOS and PN spectra were found to give consistent results, so the values given in this paper are those for joint fits to the instruments. A simple power-law fit over the 0.2–10 keV band showed significant curvature in all five spectra (Fig. 1). For three of the QSOs, upward curvature was found at low ($< 1\text{--}2$ keV observer’s frame) energies, indicating soft excess emission; although the panel for PG 1634+706 does not show an obvious excess of counts at lower energies, it was found to be better fitted by the inclusion of a soft excess component (see Section 3.2).

Table 1. Information about the observations and *XMM-Newton* configurations for the QSOs.

Object	Obs. ID	Obs. date (rev.)	Exposure time (ks) ^a			Filter MOS/PN	Mode ^b		
			MOS 1	MOS 2	PN		MOS 1	MOS 2	PN
Q 0144–3938	0090070101	2002/06/18 (0462)	32.3	32.3	28.1	Medium	lw	lw	ff
UM 269	0090070201	2002/01/05 (0380)	20.3	20.3	16.3	Medium	lw	lw	ff
PG 1634+706	0143150101	2002/11/22 (0541)	13.7	13.7	12.6	Medium	ff	ff	ff
SBS 0909+532 ^c	0143150301	2003/04/17 (0614)	12.9	12.9	10.7	Medium	ff	ff	ff
	0143150601	2003/05/18 (0630)	17.0	17.1	13.8	Medium	ff	ff	ff
PG 1247+267	0143150201	2003/06/18 (0645)	24.0	24.0	19.0	Medium	ff	ff	ff

^a‘Clean’ exposure times are given, after excluding periods of high background flares.

^bHere, lw denotes large window, ff denotes full-frame.

^cThis first observation of SBS 0909+532 was wiped out due to high background.

Table 2. Information about the five QSOs in this sample. $E(B-V)$ values are taken from the NED. The radio fluxes were measured at 1.5 GHz. (i) NRAO/VLA Sky Survey (Condon et al. 1998); (ii) Wadadekar & Kembhavi (1999); (iii) Vignali et al. (1999); (iv) Barvainis, Lonsdale & Antonucci (1996); (v) Reeves & Turner (2000); (vi) FIRST survey (Becker, White & Helfand 1995); (vii) Kellerman et al. (1989).

Object	RA J2000	Dec. J2000	Redshift	Galactic N_H (10^{20} cm^{-2})	$E(B-V)$	Radio flux density (mJy)	R_L	Reference
Q 0144–3938	01:46:12.5	–39:23:5.0	0.244	1.44	0.014	2.5	<0.2	(i)
UM 269	00:43:19.7	00:51:15.0	0.308	2.30	0.02	1.1	0.67	(ii), (iii)
PG 1634+706	16:34:28.9	70:31:33	1.334	4.48	0.04	1.65	–0.59	(iv), (v)
SBS 0909+532	09:13:1.6	52:59:29.1	1.376	1.6	0.015	1.09	–0.92	(vi)
PG 1247+267	12:50:5.6	26:31:9.8	2.038	0.9	0.013	1.17	0.36	(vii)

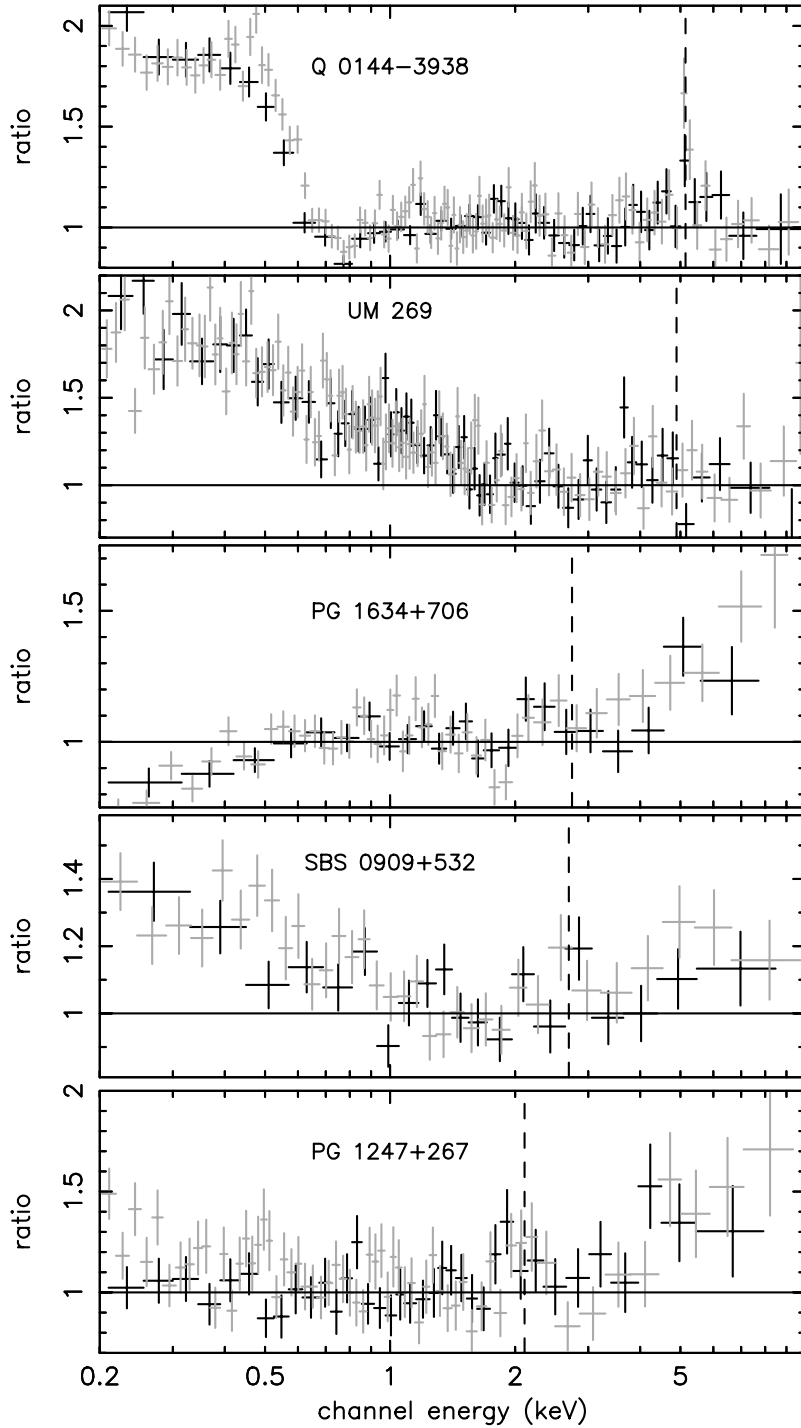


Figure 1. The plots show the ratio of the data to a power-law model, fitted over 2–10 keV in the rest frame. Extrapolating the power-law fit over 0.2–10 keV (observer’s frame) shows soft excesses in three of the objects; in the spectrum of PG 1247+267 the reflection component is dominant. The vertical dotted line marks the position of 6.4 keV in the rest frame. Positive residuals can be identified in the spectra of Q 0144–3938, PG 1247+267 and SBS 0909+532, indicating the presence of iron emission. Co-added MOS residuals are shown in black, PN in grey.

The last panel of Fig. 1 (PG 1247+267) shows an excess of counts in the high-energy portion of the spectrum. To avoid the curvature, the spectra over the rest-frame 2–10 keV bands were initially investigated. First, a power-law model, attenuated by neutral absorption, was tried, where N_{H} was fixed at the Galactic value for each object, calculated using the N_{H} FTOOL (Dickey & Lockman 1990). Next a Gaussian component was included for each spectrum, to measure emission from Fe $K\alpha$; if such a line was insignificant, then only the

upper limit on the equivalent width (EW) is quoted in Table 3. As the table shows, two of the objects did not require any iron emission components. The remaining three QSOs, however, did show significant evidence for neutral Fe K emission, at >99 per cent confidence, according to an F-test.

Allowing the width of the line in Q 0144–3938 to vary improved the fit slightly over a narrow-line model (null probability of 1.7×10^{-2}); the best-fitting line was found to have an intrinsic width of

Table 3. Fits over the 2–10 keV energy band; 90 per cent errors (Q 0144–3938, SBS 0909+532 and PG 1247+267) and upper limits (UM 269 and PG 1634+706) are given for the EW of the iron line. The width of the lines have been corrected to the rest frame of the objects in question. The F-test null probability compares the fit with the iron line to that with only the power law, with the number of extra free parameters in brackets.

Object	Fit	Model	Γ	Line energy (keV)	σ (keV)	Equivalent width (eV)	χ^2/dof	F-test null prob. (free param.)
Q 0144–3938	1	PL	1.78 ± 0.05				343/369	
	2	PL+GA	1.82 ± 0.05	6.45 ± 0.06	0.15 ± 0.1	215 ± 80	317/366	2.36×10^{-6} (3)
UM 269	1	PL	1.68 ± 0.10				211/198	
	2	PL+GA	1.69 ± 0.10	6.4^f	0.01^f	<80	210/197	0.334 (1)
PG 1634+706	1	PL	2.19 ± 0.05				285/296	
	2	PL+GA	2.19 ± 0.05	6.4^f	0.01^f	<72	284/295	0.309 (1)
SBS 0909+532	1	PL	1.71 ± 0.05				205/227	
	2	PL+GA	1.73 ± 0.06	6.42 ± 0.11	<0.49	200 ± 75	196/224	6.41×10^{-3} (3)
PG 1247+267	1	PL	2.15 ± 0.07				123/160	
	2	PL+GA	2.23 ± 0.10	6.30 ± 0.36	0.52 ± 0.35	421 ± 215	112/157	2.04×10^{-3} (3)

$\sigma \sim 0.15$ keV. The spectrum of SBS 0909+532 also showed evidence for a line, but it was not possible statistically to differentiate between a narrow and a broadened component; hence, the 90 per cent upper limit to the width is given in Table 3. Finally, PG 1247+267 showed iron emission as well. This line was also better modelled with a broad component, with an EW of ~ 400 eV for a width of $\sigma \sim 0.52$ keV (decrease in χ^2/dof of 5/1, compared to a narrow line; the F-test null probability for this is 8.9×10^{-3}). It should be noted that Protassov et al. (2002) have shown that the F-test may not be an appropriate statistic for determining the significance of marginal line parameters and should be used with caution. Thus, although there is evidence that the iron line may be broadened, no definite statement can be made.

None of the five QSO spectra showed any evidence for iron absorption edges at $\gtrsim 7$ keV, in contrast to PDS 456, for example (Reeves, O’Brien & Ward 2003), which is also a high-luminosity radio-quiet AGN.

3.2 Broad-band X-ray continuum

Because three of the QSOs in this sample are at $z > 1$, the presence of a Compton reflection hump was investigated, using the model PEXRAV (Magdziarz & Zdziarski 1995) in XSPEC. In the standard model of AGN, reflection can occur from the accretion disc and/or molecular torus (e.g. Lightman & White 1988; George & Fabian 1991). At $z = 1$, the *XMM-Newton* band extends up to 20 keV in the rest frame, so it might be expected that any spectral flattening due to reflection would be observable. Because reflection components can also affect the lower-energy spectra, these fits were conducted over the full 0.2–10 keV energy band. The results of this model, given in Table 4, show that only in PG 1247+267 was a reflection component significantly detected; upper limits are given for the remaining four objects. For PG 1247+267, a simple power-law plus Gaussian fit over the broad-band gave a reduced χ^2 value of 270/295; the inclusion of the reflection parameter decreased this to 236/294, giving a null probability of 3.3×10^{-10} . The component in PG 1247+267 is strong, with $R \sim 2$, and is required in addition to the broad line; R is defined to be $\Omega/2\pi$, where Ω is the solid angle subtended by the scattering medium. Thus, for a value of $R > 1$, the indication is that reflection is occurring from $>2\pi$ steradian, which is unphysical; possible explanations are discussed in Section 5.

As one would expect the strength of the Compton reflection hump to scale directly with the EW of the iron line for a given photon index and disc inclination, the iron line EW was linked to the strength

Table 4. Compton reflection fits to the data. The reflection component, modelled using PEXRAV, is given by $R = \Omega/2\pi$. These values were obtained by modelling the broad-band (0.2–10 keV) X-ray spectra of the objects. F-test probabilities are given for one additional degree of freedom.

Object	Reflection parameter	F-test null prob.
Q 0144–3938	<1.33	0.341
UM 269	<2.00	0.999
PG 1634+706	<0.72	0.567
SBS 0909+532	<1.1	0.999
PG 1247+267	2.87 ± 0.96	3.3×10^{-10}

of the reflection component, R , within the PEXRAV model. To determine the scaling between R and the line EW, the model of George & Fabian (1991) was used, appropriate for reflection off neutral matter. In the case where the continuum photon index is $\Gamma \sim 2.3$, with an inclination angle for the reflector of 30° to the line of sight, a reflection component with $R = 1$ should produce an iron line with an EW of ~ 120 eV. Refitting this reflection model to PG 1247+267 then resulted in a slightly weaker iron line, with an EW of 259 ± 74 eV, whilst the strength of the corresponding reflection component is then $R = 2.2 \pm 0.7$, consistent with the previous fit. The energy and velocity width of the line are largely unchanged, with $E = 6.35 \pm 0.51$ keV and $\sigma = 0.53 \pm 0.37$ keV. The reflection component is clearly detected in Fig. 1, with a null probability of 5.4×10^{-10} (for the presence of both the line and reflection component); this corresponds to $\Delta\chi^2 = 40$ for three degrees of freedom. The reflection hump is consistent with the strong line observed and the fit with both the broad line and reflector is shown in Fig. 2. Fig. 3 shows the confidence contours for the strength of the reflection and the power-law slope, demonstrating clearly that the data are inconsistent with a reflection parameter of zero at >99 per cent.

Extrapolating the best-fitting 2–10 keV models over the full *XMM-Newton* bandpass showed obvious soft excesses (Fig. 1) in three of the five QSOs; fit 3 in Table 5 gives the reduced χ^2 value for this extrapolation. The soft excess emission appears strongest in those QSOs at the lower redshifts; however, this is mainly a selection effect, because the soft excess will be shifted out of the *XMM-Newton* energy bandpass as the redshift increases. Likewise, at higher z , any reflection component in the spectrum will be shifted into the hard band, making high-energy curvature more obvious in the data. The most straightforward, if not particularly physical,

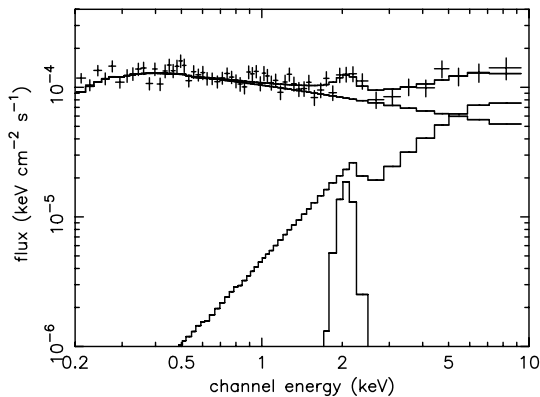


Figure 2. The best fit to the broad-band spectrum of PG 1247+267 includes a strong reflection component, as this unfolded plot shows. There is also a correspondingly strong, broad Fe K α emission line. PN data only are shown for clarity.

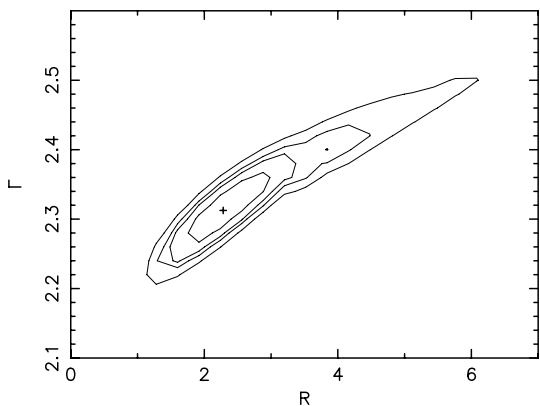


Figure 3. 68, 90, 95 and 99 per cent confidence contours (two interesting parameters) for the strength of the reflection parameter in PG 1247+267 against photon index. The data are not consistent with zero reflection.

method for modelling the soft excess is the inclusion of blackbody (BB) components. As Table 5 shows, the objects were generally best fitted with one or two BBs in addition to the power law (fits 5 and 6); however, the fit to Q 0144–3938 improves enormously with the addition of a warm absorber component (modelled with `ABSOR1` in `XSPEC`), in the rest frame of the AGN. The presence of this component was suggested in Fig. 4 by a dip in the spectrum around 0.6–0.8 keV. The main component of this warm absorber are edges corresponding to O VII and O VIII. The other QSOs showed no evidence for excess N_{H} and upper limits for cold absorption are given in Table 5. It was found that there was only weak evidence for a soft emission component in PG 1247+267, with the reflection component accounting for most of the spectral curvature. Alternatively, the spectral shape of PG 1247+267 can be modelled by a much flatter power law, together with three BB components and the broad line, but no Compton reflection hump. For $\Gamma = 1.61 \pm 0.14$ and BB temperatures of $kT = 0.067 \pm 0.014$, 0.267 ± 0.045 and 0.702 ± 0.089 keV, a χ^2 value of 229 for 288 degrees of freedom is obtained. However, this model is inconsistent with the presence of the strong emission line, which is an indication that a reflection component should be present (assuming the reprocessing medium is Compton-thick).

An alternative method for modelling the curvature is using a broken power law to model the entire spectrum; these fits are quoted in Table 6. For four of the QSOs, the break energies for the broken

power law (given in the rest frame) are 1–4 keV, indicative of modelling soft excess emission; PG 1247+267 shows spectral hardening at higher energies, which is more suggestive of reflection, agreeing with the previous fits. Only the spectrum of SBS 0909+532 can be fitted statistically as well with a broken power law as with the power-law/BB model. However, for the case of PG 1634+706, including an additional rest-frame absorption component [$N_{\text{H}} = (16 \pm 2) \times 10^{20} \text{ cm}^{-2}$] actually improves the fit, despite there being no evidence for such absorption when modelling the spectrum with a power law and BB. BB spectra curve over at lower energies, while power laws do not; Fig. 1 shows that the spectrum of PG 1634+706 does roll over slightly at the low energies, hence the requirement for the excess absorption. This fit results in $\chi^2/\text{dof} = 487/506$, a decrease of 7 for one degree of freedom, compared to the BB fit. UM 269, SBS 0909+532 and PG 1247+267 still show no sign of an increased column density.

Table 7 lists the 2–10 and 0.2–10 keV fluxes and unabsorbed luminosities, derived from the best-fitting power-law/BB models. Note that SBS 0909+532 is a gravitational lens (Kochanek et al. 1997; Oscoz et al. 1997; Lehár et al. 2002); hence, the luminosity estimated from the fits is much too high. Chartas (2000) has estimated that the luminosity of this object is enhanced by a factor of 15, thus the values determined from fitting the X-ray spectrum have been scaled down by this amount in the tables and figures in this paper.

Although blackbodies parametrize the soft excess very well, the temperatures for these components are significantly hotter than could be feasibly expected from a luminous QSO accretion disc. There is a relationship between the disc temperature, accretion rate and the mass of the black hole, given by (Peterson 1997):

$$T(r) \sim 6.3 \times 10^5 \left(\frac{\dot{M}}{M_{\text{Edd}}} \right)^{1/4} M_8^{-1/4} \left(\frac{r}{R_{\text{sch}}} \right)^{-3/4} \text{ K.} \quad (1)$$

For a black hole mass of $\sim 10^9 M_{\odot}$, the hottest temperature (i.e. at an innermost radius of $3 R_{\text{sch}}$, where the Schwarzschild radius $R_{\text{sch}} = 2GM/c^2$) is ~ 10 eV. The temperatures found by fitting the soft excess with BB components (Table 5) are much higher than this, generally with $kT \gtrsim 100$ eV. This indicates that the excess seen is not due to direct thermal emission from the accretion disc and requires Compton up-scattering of the disc photons.

Inverse Comptonization of the thermal photons can form both the soft excess and the apparent hard X-ray power law. This theory suggests that there is a population of hot electrons, above the disc,

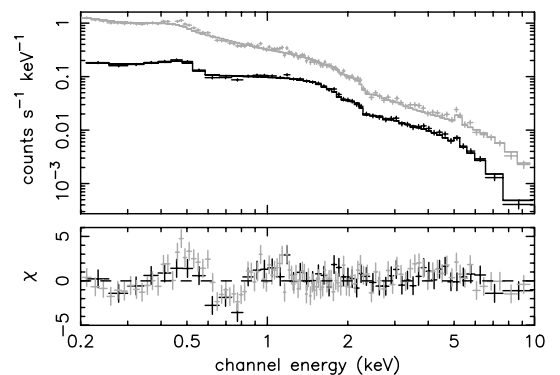


Figure 4. After modelling the broad-band spectrum of Q 0144–3938 with a power law, two BBs and an iron line, a dip can be seen in the spectrum around 0.6–0.8 keV (observer’s frame); this indicates the presence of the warm absorber. MOS data are plotted in black, PN in grey.

Table 5. Fits over the 0.2–10 keV energy bands; the F-test values are given for each BB model compared to the previous fit. The Fe lines present in Q 0144–3938, SBS 0909+267 and PG 1247+267 were fixed to the values determined over the 2–10 keV band. The ‘EXTRAP.PL’ fit refers to the χ^2 value obtained if the power law fitted to the 2–10 keV rest frame is simply extrapolated over the full 0.2–10 keV band. The fits for PG 1247+267 also include a reflection component, REF (see Table 4).

Object	Fit	Model	Γ	kT^a (keV)	kT^a (keV)	N_{H}^b (10^{20} cm^{-2})	ξ^c	χ^2/dof	F-test null probability
Q 0144–3938	3	EXTRAP. PL	1.82 ± 0.05					3289/754	
	4	PL	2.07 ± 0.05					2112/754	
	5	PL+BB	1.74 ± 0.04	0.095 ± 0.003				956/752	1.00×10^{-99}
	6	PL+2BB	1.54 ± 0.07	0.103 ± 0.003	0.488 ± 0.030			902/750	3.39×10^{-10}
	7	(PL+2BB)*ABS	1.81 ± 0.05	0.123 ± 0.008	0.283 ± 0.020	97 ± 29	98 ± 32	828/748	1.25×10^{-14}
UM 269	3	EXTRAP. PL	1.68 ± 0.10					1824/514	
	4	PL	1.93 ± 0.03					621/514	
	5	PL+BB	1.84 ± 0.04	0.120 ± 0.016				564/512	1.97×10^{-11}
	6	PL+2BB	1.59 ± 0.10	0.104 ± 0.011	0.311 ± 0.035	<8		533/510	5.49×10^{-7}
PG 1634+706	3	EXTRAP. PL	2.19 ± 0.05					606/509	
	4	PL	2.11 ± 0.02					548/509	
	5	PL+BB	1.96 ± 0.05	0.404 ± 0.027		<7		494/507	3.79×10^{-12}
SBS 0909+532	3	EXTRAP. PL	1.73 ± 0.06					514/428	
	4	PL	1.81 ± 0.01					424/428	
	5	PL+BB	1.64 ± 0.05	0.274 ± 0.034				375/426	4.36×10^{-12}
PG 1247+267	6	PL+2BB ^d	1.60 ± 0.04	0.102 ± 0.039	0.335 ± 0.038	<1		367/424	1.00×10^{-2}
	3	EXTRAP. PL	2.23 ± 0.10					287/295	
	4	PL	2.18 ± 0.02					270/295	
	4.5	PL+REF	2.34 ± 0.04					236/293	2.73×10^{-9}
	5	PL+REF+BB ^d	2.30 ± 0.05	0.050 ± 0.020		<9		230/291	2.00×10^{-2}

^aBB temperature.

^bAbsorption component.

^cIonization of the warm absorber.

^dThis soft emission component is only marginally significant.

Table 6. Broken power-law fits to the broad-band spectra; absorption/Gaussian components are included as before. Γ_{soft} is the photon index below the break energy (E_{break}), Γ_{hard} above. The break energy is given in the QSO rest frames. The final column gives the change in χ^2/dof between the broken power-law fits and power-law/BB model; a negative sign demonstrates that the χ^2 value is lower for the BB fit.

Object	Fit	Model	Γ_{soft}	E_{break}	Γ_{hard}	χ^2/dof	$\Delta\chi^2/\text{dof}$
Q 0144–3938	8	BKNPL	2.20 ± 0.03	3.35 ± 0.76	1.82 ± 0.06	848/750	–20/2
UM 269	8	BKNPL	2.07 ± 0.03	2.68 ± 0.43	1.65 ± 0.08	544/512	–11/2
PG 1634+706 ^a	8	BKNPL	2.12 ± 0.01	1.63 ± 0.38	1.84 ± 0.17	541/507	–47/1
SBS 0909+532	8	BKNPL	1.95 ± 0.05	3.80 ± 0.81	1.58 ± 0.08	368/426	–1/2
PG 1247+267	8	BKNPL	2.24 ± 0.04	7.93 ± 1.73	1.63 ± 0.24	239/293	–9/2

^aSee text for an alternative fit, including absorption.

Table 7. Fluxes and luminosities over the 2–10 keV (rest frame) and 0.2–10 keV (observer’s frame) energy bands, calculated from the power-law plus BB models. The luminosities of SBS 0909+532 have been decreased by a factor of 15 due to the object being a gravitational lens; the fluxes, however, are the actual observed values. The sixth column gives the rest-frame energy range to which the *XMM-Newton* band of 0.2–10 keV corresponds. The bolometric luminosities (estimated from 2500 Å) and (lower-limit) black hole masses are also quoted.

Object	2–10 keV (rest-frame)		0.2–10 keV (observer’s frame)		Rest frame <i>XMM-Newton</i> band	Bolometric luminosity (erg s ^{–1})	Black hole mass (M_{\odot})
	Flux (erg cm ^{–2} s ^{–1})	Luminosity (erg s ^{–1})	Flux (erg cm ^{–2} s ^{–1})	Luminosity (erg s ^{–1})			
Q 0144–3938	1.21×10^{-12}	2.32×10^{44}	2.58×10^{-12}	6.60×10^{44}	0.25–12.44	2×10^{46}	2×10^8
UM 269	8.90×10^{-13}	2.80×10^{44}	1.92×10^{-12}	6.54×10^{44}	0.26–13.08	7×10^{45}	5×10^7
PG 1634+706	1.16×10^{-12}	1.32×10^{46}	2.98×10^{-12}	3.30×10^{46}	0.47–23.34	2×10^{48}	1×10^{10}
SBS 0909+532	3.70×10^{-13}	5.18×10^{44}	1.53×10^{-12}	1.29×10^{45}	0.48–23.76	4×10^{46}	3×10^8
PG 1247+267	6.00×10^{-14}	9.21×10^{45}	7.00×10^{-13}	2.78×10^{46}	0.61–30.38	1×10^{48}	1×10^{10}

which Comptonizes the disc photons to produce the observed soft excess. The ‘power law’ at higher energies could also be formed by Comptonization, but through interactions with a much hotter electron corona. Comptonized spectra ‘roll over’ at $\sim 4kT$; hence, for a relatively cool (<1 keV, say) electron population, the component will be similar in shape to a BB, only somewhat broader. For a hot

electron population (~ 100 keV), the spectrum will appear power-law-like out to energies well beyond the energy bandpass of most current X-ray instruments.

The Comptonization model used to fit these spectra was THCOMPFE (Zdziarski, Johnson & Magdziarz 1996); the results are shown in Table 8 and the fits in Fig. 5. The temperature of the hottest

Table 8. Double-Comptonization fits to the data. The absorption component was included for Q 0144–3938. kT_{bb} is the input BB temperature, kT_e is the electron temperature, τ is the optical depth, and the superscript ‘f’ denotes frozen.

Object	Fit	Model	Cooler Comptonized component			Hotter Comptonized component			χ^2/dof
			$kT_{\text{bb}}^{\text{f}}$ (eV)	kT_e (keV)	τ	$kT_{\text{bb}}^{\text{f}}$ (eV)	kT_e^{f} (keV)	Γ	
Q 0144–3938	9	2THCOMPFE	20	0.261 ± 0.016	32 ± 4	20	200	1.90 ± 0.04	836/749
UM 269	9	2THCOMPFE	30	0.496 ± 0.168	13 ± 3	30	200	1.62 ± 0.09	544/512
PG 1634+706	9	2THCOMPFE	10	0.420 ± 0.060	40 ± 18	10	200	1.95 ± 0.05	541/506
SBS 0909+532	9	2THCOMPFE	10	0.491 ± 0.169	15 ± 5	10	200	1.60 ± 0.05	368/425

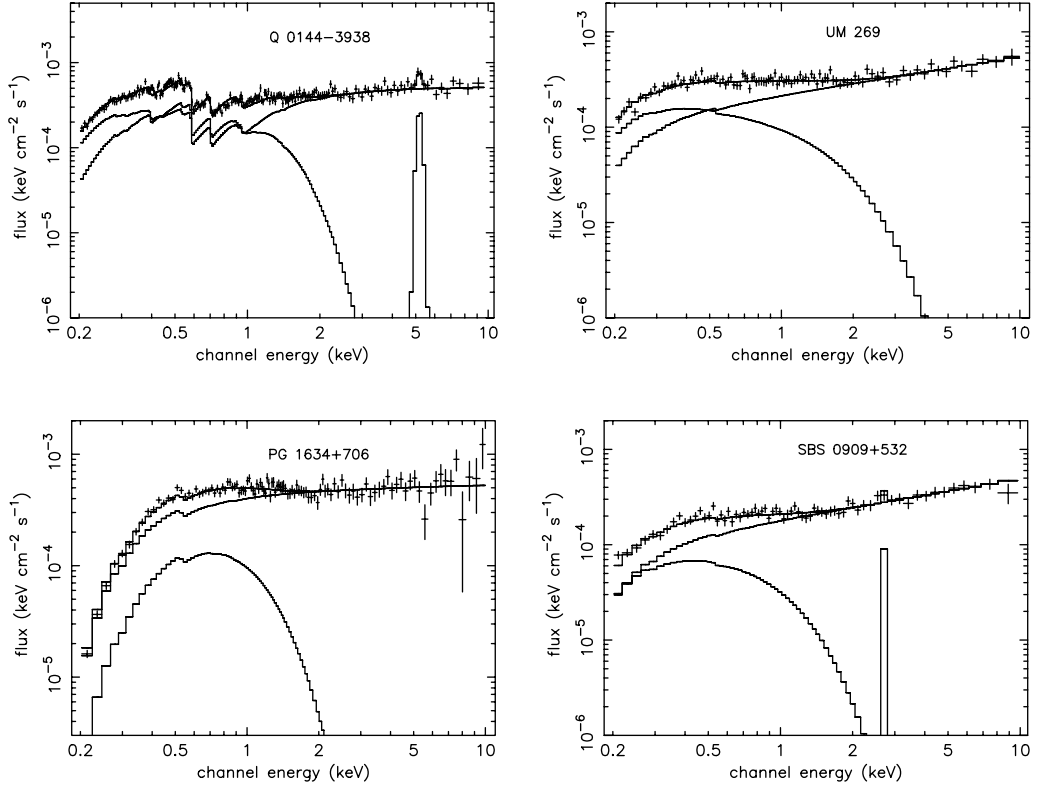


Figure 5. Unfolded plots showing the Comptonization fits to the spectra of Q 0144–3938, UM 269, PG 1634+706, SBS 0909+532 and PG 1247+267. As before, Q 0144–3938 includes additional absorption.

Comptonizing distribution was set to 200 keV, because the roll-off for the ‘power-law’ component is expected to be outside the bandpass of *XMM–Newton*, as explained above. This component will appear very similar to a power law over this limited energy band. Modelling the spectra with an actual power law (with a Comptonization component for the soft excess) leads to almost identical fits; Comptonization of the disc photons by hot electrons is, however, a plausible explanation for the formation of the observed power-law emission. The model for Q 0144–3938 includes a similar value for excess absorption as for the BB fit. The temperature of the disc photons will be cooler than can easily be modelled over the *XMM–Newton* band. Subsequently, an estimate of the accretion disc temperature was made as follows. The luminosity at 2500 Å (rest frame) was estimated from the *V*-band magnitude assuming a slope of 0.7; from Elvis et al. (1994), a typical QSO has a median bolometric to 2500-Å luminosity ratio of $L_{\text{Bol}}/L_{2500\text{Å}}$ of 5.6. This allowed an estimate of the black hole mass to be obtained (Table 7), because

$$L_{\text{Edd}} = \frac{4\pi GM_{\text{p}}c}{\sigma_{\text{T}}} \approx 1.3 \times 10^{38} \frac{M}{M_{\odot}} \text{erg s}^{-1}. \quad (2)$$

This estimate will be a lower limit to the mass, because it has been assumed that accretion occurs at the maximum Eddington rate. Taking an accretion rate of \dot{M}_{Edd} to be a typical value for high-luminosity QSOs, the temperature of the disc was calculated for each object, for a radius of $3 R_{\text{sch}}$, using equation (1). The resultant temperatures were rounded to the nearest 5 eV, and are listed in the fourth column of Table 8.

Two comments must be made about these Comptonization fits. First, the resulting model was largely insensitive to the estimated disc temperatures, because they are so low. Secondly, the geometry of AGN is unknown: it could be that some disc photons are Comptonized to soft excess energies, while others directly interact with the hotter electron population, forming the hard power law. Alternatively, the two Comptonizing electron populations could be ‘layered’, such that some photons are first Comptonized by the warm, ‘soft excess’ population, before undergoing further Comptonization with the hotter electron cloud (due to the disc corona). If this were to be the case, then the input temperatures for the two components should not be the same. The results given in Table 8 assume the first of these possible scenarios. The fits were

also tried allowing the input photons to the hotter Comptonizing electrons to have a varying temperature; however, statistically the fits could not be differentiated for these spectra. Because it was found earlier that the spectrum of PG 1247+267 could be well described without a soft excess component if reflection were included, these data were not modelled with the Comptonization components.

4 OPTICAL MONITOR DATA

With the exception of UM 269, OM observations were obtained for the AGN in this sample; Table 9 lists the magnitudes found in each band. Also given is α_{ox} , the two-point optical to X-ray spectral index. As for estimating the bolometric luminosity, a typical optical slope of 0.7 ($f_{\nu} \propto \nu^{-0.7}$) was assumed, to convert the OM UV flux at 2120 Å (observer's frame; for UM 269, the V-band flux at 5500 Å was used) to an estimate of the value at 2500 Å (in the rest frame), needed for the definition of α_{ox} , which is

$$\alpha_{\text{ox}} = \frac{\log[f_{\nu}(2 \text{ keV})/f_{\nu}(2500 \text{ \AA})]}{\log[\nu(2 \text{ keV})/\nu(2500 \text{ \AA})]} \quad (3)$$

Spectral energy distributions (SEDs) were produced, showing the Comptonization fit over the *XMM-Newton* band, together with the OM optical/UV points; these are plotted in Fig. 6. There is an added complication for the objects at higher redshift, however. For PG 1634+706, SBS 0909+532 and PG 1247+267, some of the OM data points are very close to the Lyman limit of 912 Å; a vertical dotted line indicates 912 Å in Fig. 6. Without applying a correction factor, the optical/UV data points would be seen to fall with increasing frequency, because some of the higher-frequency photons have been absorbed. Barvainis (1990) plots an SED for PG 1634+706 at frequencies lower than $\sim 2 \times 10^{15}$ Hz, where the spectrum can be seen to be rising as the frequency increases. Similarly, Koratkar, Kinney & Bohlin (1992) show a UV spectrum of PG 1247+267, where absorption below ~ 2000 Å can clearly be seen. The measurements which fall between Ly α (1216 Å) and Ly β (1026 Å), or between Ly β and the limit of the series, have been corrected by the mean values for the Lyman line absorption given by O'Brien, Gondhalekar & Wilson (1988). Beyond the Lyman limit, absorption by the continuum is also important. This correction factor is, however, uncertain, so the two highest-frequency UV points in PG 1247+267 have only been corrected for the line absorption, not the additional continuum absorption; therefore, the UV spectrum in this case is reddened.

Table 9. Optical and UV magnitudes obtained from the OM. The corresponding wavelengths for the different bands are: V, 550 nm; B, 440 nm; U, 360 nm; UVW1, 291 nm; UVM2, 231 nm; UVW2, 212 nm. The last column gives the calculated two-point optical to X-ray slope, α_{ox} .

Object	Mean optical and UV magnitudes						α_{ox}
	V	B	U	UVW1	UVM2	UVW2	
Q 0144–3938	–	16.7	15.6	15.5	–	15.1	–1.47
UM 269	17.85 ^a	–	–	–	–	–	–1.40
PG 1634+706	14.8	–	14.1	–	–	14.1	–1.57
SBS 0909+532	–	–	–	15.4	15.8	15.8	–1.44
PG 1247+267	–	–	–	15.0	15.3	15.6	–1.55

^aThe V-band magnitude for UM 269 has been taken from the Hewitt & Burbidge (1993) catalogue, because no OM data were obtained.

5 DISCUSSION

In this paper, optical to X-ray SEDs have been investigated for high-luminosity, RQQs, ranging from $\sim 7 \times 10^{44}$ to 3×10^{46} erg s^{–1} over the X-ray band (7×10^{45} to 2×10^{48} erg s^{–1} bolometric).

When fitting the rest-frame 2–10 keV band, the mean photon index for the five QSOs in this sample is $\Gamma = 1.93 \pm 0.02$. Despite the sample being small, this value is in very good agreement with the slopes measured in ASCA spectra by Reeves & Turner (2000), for which a mean slope of 1.89 ± 0.05 was found for the RQQs, and also with *Ginga* results (Lawson & Turner 1997). Similarly, Page et al. (2003) also obtained an average value of 1.89 ± 0.04 , for a sample of lower-luminosity serendipitous *XMM-Newton*-detected QSOs. This value of $\Gamma \sim 1.9$ is the same as that found for Seyfert 1 galaxies by Nandra & Pounds (1994). The mean α_{ox} for this sample was found to be -1.48 . This is somewhat flatter than other surveys of QSOs have found: e.g. 1.66 (Page et al. 2003); 1.56–1.78 (Vignali et al. 2001). However, the result is not surprising, because the five objects in this sample were selected from luminous AGN in the *ROSAT* All-Sky Survey and are, therefore, X-ray bright. α_{ox} has been previously found to become steeper with increased luminosity (e.g. Wilkes et al. 1994; Vignali, Brandt & Schneider 2003). This small sample confirms these results, with a simple Spearman Rank correlation giving a probability of 98 per cent.

The vast majority of luminous AGN (Turner & Pounds 1989; Pounds & Reeves 2002) show soft excesses, i.e. emission above the extrapolation of a power law, fitted to the 2–10 keV (rest-frame) energy band, at energies $\lesssim 1$ keV. Four of the QSOs in this sample show soft excess emission very clearly; the evidence is only marginal for PG 1247+267, where the reflection component provides the observed curvature in the spectrum at higher energies. It should be noted that, at higher redshifts, cool soft excesses will become more difficult to detect, due to the shift in the rest-frame energy band to higher values. PG 1247+267 shows a weak indication for a BB component of $kT \sim 50$ eV, which, at $z = 2.038$, is mainly shifted out of the bandpass of *XMM-Newton*. Alternatively, if the spectrum is modelled without a reflection parameter, then PG 1247+267 shows a very hot soft excess (highest BB kT of ~ 0.7 keV); this lack of reflection is not consistent with the strong iron line, though, unless the reprocessing material is Compton-thin.

Thus, it appears that high-luminosity radio-quiet AGN have identical X-ray continuum properties to lower-luminosity QSOs and Seyfert 1 galaxies. The objects in this sample cover a range of X-ray luminosities between $\sim 7 \times 10^{44}$ and 3×10^{46} erg s^{–1}, whereas Seyfert galaxies typically cover a range of $\sim 10^{42}$ – 10^{44} erg s^{–1} (Nandra & Pounds 1994). This indicates that the AGN X-ray continuum shape remains essentially constant over a wide range of black hole mass and luminosity.

Two components are required to model the broad-band X-ray continuum. These can be explained through Comptonization of photons from the accretion disc: the hard X-ray power law is produced through an interaction with hot (possibly non-thermal) electrons in a corona above the accretion disc. A second, cooler population of electrons (~ 0.5 keV, rather than >100 keV) produces the soft excess; these electrons are still much hotter than the accretion disc itself, though, which has a temperature of $kT \lesssim 30$ eV. It is not yet clear how the soft excess electrons are heated. One possibility is that some areas of the accretion disc are irradiated by the hot electron corona; this could lead to ‘hotspots’ on the accretion disc, where a warm, mildly ionized layer could Comptonize the thermal optical/UV photons to the soft excess temperatures (e.g. di Salvo et al. 2001). Alternatively, the regions of the disc heated by the

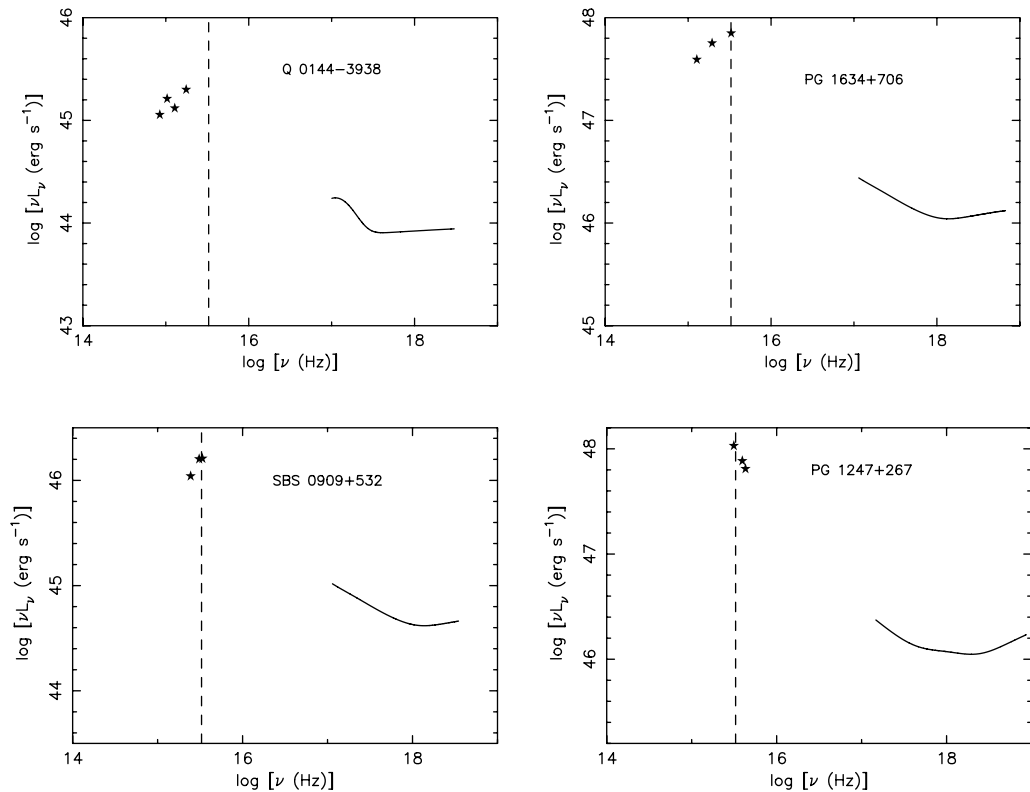


Figure 6. SEDs plotting the EPIC and (dereddened) OM data. The vertical dotted line signifies the Lyman limit (912 \AA). The abscissa gives the frequency in the rest frame. The EPIC data were modelled with two THCOMP components, and the unabsorbed data have been plotted. The OM points (shown as stars) have been dereddened and corrected for Lyman line absorption. Note, however, that the two points at higher frequencies than the Lyman limit in PG 1247+267 have only been corrected for absorption due to the Lyman lines, not the Lyman continuum as well; they are, therefore, too red.

flares could thermalize the radiation, forming a BB spectrum with a temperature higher than that of the mean disc emission (Haardt, Maraschi & Ghisellini 1994). The size of this soft-excess-forming ‘region’ can be estimated by assuming that the emission is BB in nature (because $\tau \gg 1$, this is a valid approximation); taking the emitting region to be circular, and performing this calculation, leads to a radius of $\sim 10^{11}–10^{12}$ m. For a black hole of mass $10^9 M_{\odot}$, the Schwarzschild radius is $\sim 3 \times 10^{12}$ m, i.e. the emitting region is actually smaller than R_{sch} . This implies that the warmer region is patchy, rather than covering the entire surface of the disc; likewise, the hot, flaring (coronal) regions must also be small. This result is also consistent with some of the disc photons being observed directly as the optical/UV emission, while yet more interact with the hot electron corona to form the observed power law.

Iron lines were commonly identified in AGN spectra by *Ginga* observations (Pounds et al. 1989, 1990; Nandra et al. 1991; Nandra & Pounds 1994). With the improved resolution of current instruments, it is sometimes possible to differentiate between narrow (< 10 eV; unresolved by an instrument such as *XMM–Newton*) and broad lines. To date, few broad lines have been found in *XMM–Newton* spectra of AGN, examples being Q 0056–363 (Porquet & Reeves 2003), MCG–5–23–16 (Dewangan, Griffiths & Schurch 2003), MCG–6–30–15 (Fabian et al. 2002b), Mrk 205 (Reeves et al. 2001) and Mrk 509 (Pounds et al. 2001). Nandra et al. (1997) reported a Baldwin effect for the broad lines in *ASCA* data – that is, as the X-ray luminosity of the source increases, the strength of the broad line diminishes. The same Baldwin effect has been identified for the narrow iron lines in *XMM–Newton* observations (Page

et al. 2004a). Also, both Reeves et al. (1997) and Lawson & Turner (1997) found that reprocessed features (such as the iron $K\alpha$ line and reflection humps) were less common in QSOs than in the lower-luminosity Seyferts. Thus, it is rather surprising to find a strong, apparently broad line, together with a clear reflection component, in such a luminous QSO as PG 1247+267 (broad-band X-ray luminosity of $\sim 2 \times 10^{46} \text{ erg s}^{-1}$). Both the strength and velocity width of the line ($\sigma = 30\,000 \text{ km s}^{-1}$) imply that the reflection is occurring off the inner accretion disc, rather than distant matter, such as the torus. The line is also much stronger than the narrow component of the Fe lines observed from further out (that is, from the broad or narrow line regions, or the torus) in many Seyfert 1s; these narrow lines are typically around 100 eV in EW (e.g. Kaspi et al. 2001; Pounds et al. 2001; Reeves et al. 2001; Page et al. 2004a). Q 0144–3938 was also better fitted with a broad, rather than a narrow line, but is less luminous than PG 1247+267; it was not possible to determine whether the line in the spectrum of SBS 0909+267 was broad or narrow. 3C 273, a luminous radio-loud quasar, has previously been reported to show evidence for a broad line (Yaqoob & Serlemitsos 2000; Page et al. 2004b), although much weaker than in PG 1247+267, with an EW of ~ 50 eV. PG 1247+267 seems to be the most luminous QSO to show a strong (apparently) broad line to date, although there is some uncertainty about whether the line is truly broad; the object also reveals the first clear detection of a reflection component in a high-luminosity AGN.

Reeves & Turner (2000) found, in a sample of 62 QSOs (both radio-loud and radio-quiet), that approximately half of the iron emission lines seen were at energies > 6.4 keV, implying the lines

originated from partially ionized matter. It seems somewhat unusual that the lines reported in this paper appear neutral; however, the current sample of five (three detections) is much smaller than in the Reeves & Turner (2000) paper.

It should be noted that the reflection component found in PG 1247+267 is very strong, even for an accretion disc: $R > 2$ implies the reflection is occurring from $>4\pi$ steradian. There are a number of possible explanations for this. It could be a geometrical phenomenon; i.e. part of the direct, hard X-ray emission may be being obscured by structure within the disc. In this case, the reflection would appear enhanced (see, for example, Fabian et al. 2002a). Alternatively, it could be due to relativistic effects. Fabian & Vaughan (2003) use gravitational light-bending as an argument for explaining the very strong line (also ~ 400 – 500 eV) observed in MCG-6-30-15.

With the discovery of such a strong iron line and reflection component in PG 1247+267, a much longer observation of the object (>19 ks of PN time as presented here) is desirable, in order to investigate the spectral features more thoroughly, including whether the line varies over time.

ACKNOWLEDGMENTS

The work in this paper is based on observations with *XMM-Newton*, a European Space Agency (ESA) science mission, with instruments and contributions directly funded by ESA and the National Aeronautics and Space Administration (NASA). The authors would like to thank the EPIC Consortium for all their work during the calibration phase, and the SOC and SSC teams for making the observation and analysis possible. This research has made use of the NASA/IPAC Extragalactic Database (NED), which is operated by the Jet Propulsion Laboratory, California Institute of Technology, under contract with NASA.

REFERENCES

Barvainis R., 1990, *ApJ*, 353, 419
 Barvainis R., Lonsdale C., Antonucci R., 1996, *AJ*, 111, 1431
 Becker R. H., White R. L., Helfand D. J., 1995, *ApJ*, 450, 559
 Chartas G., 2000, *ApJ*, 531, 81
 Condon J. J., Cotton W. D., Greisen E. W., Yin Q. F., Perley R. A., Taylor G. B., Broderick J. J., 1998, *AJ*, 115, 1693
 Dewangan G. C., Griffiths R. E., Schurch N. J., 2003, *ApJ*, 592, 52
 Dickey J. M., Lockman F. J., 1990, *ARA&A*, 28, 215
 di Salvo T., Done C., Życki P. T., Burderi L., Robba N. R., 2001, *ApJ*, 547, 1024
 Elvis M. et al., 1994, *ApJS*, 95, 1
 Fabian A. C., Vaughan S., 2003, *MNRAS*, 340, L28
 Fabian A. C., Ballantyne D. R., Merloni A., Vaughan S., Iwasawa K., Boller Th., 2002a, *MNRAS*, 331, L35
 Fabian A. C. et al., 2002b, *MNRAS*, 335, L1
 George I. M., Fabian A. C., 1991, *MNRAS*, 249, 352
 Haardt F., Maraschi L., Ghisellini G., 1994, *ApJ*, 432, L95
 Hewitt A., Burbidge G., 1993, *ApJS*, 87, 451
 Kaspi S. et al., 2001, *ApJ*, 554, 216
 Kellerman K. I., Sramek R., Schmidt M., Shaffer D. B., Green R., 1989, *AJ*, 98, 1195

Kochanek C. S., Falco E. E., Schild R., Dobrzycki A., Engels D., Hagen H.-J., 1997, *ApJ*, 479, 678
 Koratkar A. P., Kinney A. L., Bohlin R. C., 1992, *ApJ*, 400, 435
 Kukula M. J., Dunlop J. S., Hughes D. H., Rawlings S., 1998, *MNRAS*, 297, 366
 Lawson A. J., Turner M. J. L., 1997, *MNRAS*, 288, 920
 Lehár J. et al., 2002, *ApJ*, 536, 584
 Lightman A. P., White T. R., 1988, *ApJ*, 335, 57
 Magdziarz P., Zdziarski A. A., 1995, *MNRAS*, 273, 837
 Nandra K., Pounds K. A., 1994, *MNRAS*, 268, 405
 Nandra K., Pounds K. A., Stewart G. C., George I. M., Hayashida K., Makino F., Ohashi T., 1991, *MNRAS*, 248, 760
 Nandra K., George I. M., Mushotzky R. F., Turner T. J., Yaqoob T., 1997, *ApJ*, 488, L91
 O'Brien P. T., Gondhalekar P. M., Wilson R., 1988, *MNRAS*, 233, 801
 Osoz A., Serra-Ricart M., Mediavilla E., Buitrago J., Goicoechea L. J., 1997, *ApJ*, 491, L7
 Page K. L., Turner M. J. L., Reeves J. N., O'Brien P. T., Sembay S., 2003, *MNRAS*, 338, 1004
 Page K. L., O'Brien P. T., Reeves J. N., Turner M. J. L., 2004a, *MNRAS*, 347, 316
 Page K. L., Turner M. J. L., Done C., O'Brien P. T., Reeves J. N., Sembay S., Stuhlinger M., 2004b, *MNRAS*, 349, 57
 Peterson B. M., 1997, *An Introduction to Active Galactic Nuclei*. Cambridge Univ. Press, Cambridge
 Porquet D., Reeves J. N., 2003, *A&A*, 408, 119
 Pounds K. A., Reeves J. N., 2002, in *New Visions of the X-ray Universe in the XMM-Newton and Chandra era* (astro-ph/0201436)
 Pounds K. A., Nandra K., Stewart G. C., Leighly K., 1989, *MNRAS*, 240, 769
 Pounds K. A., Nandra K., Stewart G. C., George I. M., Fabian A. C., 1990, *Nat*, 344, 132
 Pounds K., Reeves J., O'Brien P., Page K., Turner M., Nayakshin S., 2001, 559, 181
 Protassov R., van Dyk D. A., Connors A., Kashyap V. L., Siemiginowska A., 2002, *ApJ*, 571, 545
 Reeves J. N., Turner M. J. L., 2000, *MNRAS*, 316, 234
 Reeves J. N., Turner M. J. L., Ohashi T., Kii T., 1997, *MNRAS*, 292, 468
 Reeves J. N., Turner M. J. L., Pounds K. A., O'Brien P. T., Boller Th., Ferrando P., Kendziorra E., Vercellone S., 2001, *A&A*, 365, L134
 Reeves J. N., O'Brien P. T., Ward M. J., 2003, *ApJ*, 593, L65
 Turner T. J., Pounds K. A., 1989, *MNRAS*, 240, 833
 Vignali C., Comastri A., Cappi M., Palumbo G. G. C., Matsuoka M., Kubo H., 1999, *ApJ*, 516, 582
 Vignali C., Brandt W. N., Fan X., Gunn J. E., Kaspi S., Schneider D. P., Strauss M. A., 2001, *AJ*, 122, 2143
 Vignali C., Brandt W. N., Schneider D. P., 2003, *AJ*, 125, 433
 Wadadekar Y., Kembhavi A., 1999, *AJ*, 118, 1435
 Wilkes B. J., Elvis M., 1987, *ApJ*, 323, 243
 Wilkes B. J., Tananbaum H., Worrall D. M., Avni Y., Oey M. S., Flanagan J., 1994, *ApJS*, 92, 53
 Worrall D. M., Giommi P., Tananbaum H., Zamorani G., 1987, *ApJ*, 313, 596
 Yaqoob T., Serlemitsos P., 2000, *ApJ*, 544, L95
 Zamorani G. et al., 1981, *ApJ*, 245, 357
 Zdziarski A. A., Johnson W. N., Magdziarz P., 1996, *MNRAS*, 283, 193

This paper has been typeset from a $\text{\TeX}/\text{\LaTeX}$ file prepared by the author.